7th International Symposium on Hydraulic Structures Aachen, Germany, 15-18 May 2018
ISBN 978-0-692-13277-7 DOI: 10.15142/T3B340

Sediment Motion beneath Surges and Bores

Y. Li[1] & H. Chanson[1]
[1]*The University of Queensland, School of Civil Engineering, Brisbane QLD 4072, Australia*
E-mail: h.chanson@uq.edu.au

Abstract: *Positive surges and bores can induce significant bed-load transport in estuaries and river channels. Based upon physical modelling, the present study investigated the sediment motion beneath bores on a relatively long gravel bed. The free-surface measurements at a series of locations showed that the bore shape varied during its upstream propagation. An ultra-high-speed camera captured the details of gravel motion at 1200 fps. Frame-by-frame analysis of slow-motion video movies demonstrated three basic modes of pebble motion: rotation, rolling, and saltation. More complicated pebble motion was a combination of 2 or 3 basic modes. The synchronous measurements of near-bottom velocity and bed-load material trajectories highlighted the importance of the adverse longitudinal pressure gradient and transient flow recirculation on the inception of particle motion. Long durations of gravel motion also indicated that the weak negative flow under secondary waves played some role in maintaining the upstream transient sediment transport.*

Keywords: *Positive surges, sediment motion, transient sheet flow, physical modelling.*

1. Introduction

A positive surge is an unsteady open channel flow defined as a rapid increase in water depth (Favre 1935, Henderson 1966). Engineering applications encompass rejection surges in hydropower canals, load acceptance surges in tailwater canals, and surges in water supply channels following rapid gate operation (Benet and Cunge 1971, Cunge 1975). Related natural processes include tsunami-induced bores and tidal bores (Yasuda 2010, Chanson 2011). The latter is a compression wave of tidal origin, developing in an estuary where the bathymetry amplifies the tidal range, in presence of macro-tidal conditions with low fresh water levels. Positive surges and bores constitute hydrodynamic shocks, associated with a discontinuity in terms of the pressure and velocity fields (Stoker 1957, Ligthhill 1978). The shock propagation is associated with intense unsteady turbulence (Leng and Chanson 2016), which may be responsible for major sediment scouring and advection of sediments and contaminants behind the bore front (Greb and Archer 2007, Khezri and Chanson 2012a,b, 2015). Further, the normal Reynolds stresses and turbulent kinetic energy (TKE) were observed to be consistently 10–30% higher on a mobile bed than on the same fixed bed, at the same relative bed elevation and for the same Froude number (Khezri and Chanson 2012c). To date, field and laboratory observations showed complicated interactions between mobile bed and turbulence transient, suggesting our continuing ignorance of unsteady turbulent processes.

The aim of this study was to characterise the sheet flow motion beneath a breaking bore propagating over a gravel bed and to ascertain the driving mechanisms. A physical study based upon a Froude similarity was conducted in a relatively large size facility with state-of-the-art instrumentation (ultra-high-speed video camera, acoustic Doppler velocimetry). The results showed the contribution of the longitudinal pressure gradient beneath the tidal bore, as well as the role played by large-scale vortices in terms of sediment pickup.

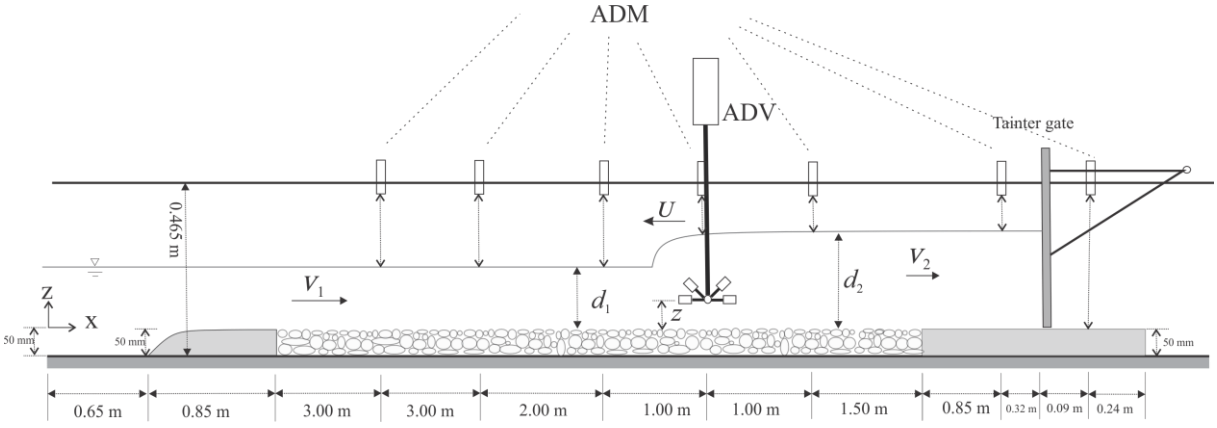

Figure 1. Experimental channel and instrumentation setup (not to scale) - V_1 and d_1: initial water velocity and depth prior to bore front; V_2 and d_2: new water velocity and depth after bore passage; U: bore celerity, positive upstream; z: vertical elevation of ADV control volume.

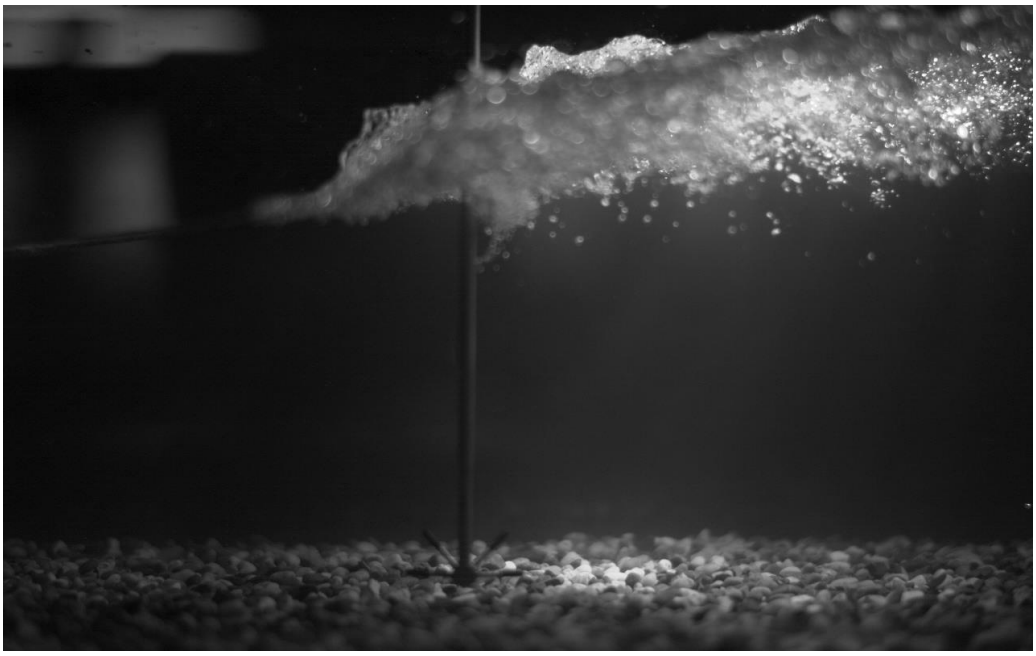

Figure 2. Breaking bore propagating upstream in the experimental channel (exposure time: 7.98 μs) - Flow conditions: Q = 0.061 m^3/s, d_1 = 0.1607 m, Fr_1 = 1.42

2. Physical Model and Instrumentation

2.1. Experimental Facility

New experiments were conducted in a 15 m long 0.495 m wide horizontal rectangular flume at the University of Queensland (Fig. 1 & 2). The flume was previously used by Yeow et al. (2016) with a smooth PVC bed. Herein, a 50 mm high smooth false floor was built at the upstream and downstream ends of the channel. In between (1.5 m < x < 13 m), the 11.5 m long 50 mm deep pit was filled with gravels (measured relative density: s = 2.5), where x is the longitudinal distance from the channel's upstream end positive downstream. The gravel materials were mixed natural river pebbles sourced from Nambucca River and Upper Brisbane River, sieved between 6.7 mm and 9.5 mm. A fast-closing gate was located at x = 14.17 m next to the channel's downstream end. The gate's rapid closure, in less than 0.2 s, generated a surge propagating upstream.

The channel was fed by a constant head reservoir supplying an upstream intake tank (1.43m×1.24m×1.0m), equipped with baffles and flow straighteners to deliver smooth inflow conditions. The intake structure was connected to the flume by a smooth three-dimensional convergent section, enabling a quasi-uniform calm inflow. The water flow rate was measured by a Venturi meter calibrated on site with an error of less than 2%. In steady flow, the water depth was measured with a pointer gauge above the top of the gravel bed, using a circular footing with a 154 cm^2 area. Unsteady water depths were measured with a series of acoustic displacement meters (ADM) Microsonic™ Mic+25/IU/TC, installed above the channel centreline and sampled at 200 Hz. The water velocities were recorded by a Nortek™ Vectrino+ acoustic Doppler velocimeter (ADV) equipped with a side-looking probe (hardware ID: VNO 0436 and VCN 7657). The ADV (firmware v1.31 +) was driven by the Vectrino+ software (v1.22.00). The vertical elevation of the ADV probe was controlled by a fine adjustment travelling mechanism connected to a HAFCO™ M733 digimatic vertical scale unit. The ADV control volume was located at x = 10.50 m on the channel centerline and z = 10.8 mm above the pebble top. The velocity range was ±1.0 m/s and the sampling rate was 200 Hz.

Observations through the right glass sidewall were recorded using a Phantom™ ultra-high-speed digital camera (v2011) equipped with a Carl Zeiss™ Planar T*85mm f/1.4 lens, producing images with negligible degree of barrel distortion (~0.209%). The camera system was capable to record up to 22,700 monochrome frames per second (fps) in high-definition (1280×800 pixels). Controlled by the PCC (Phantom Camera Control, v2.8.761.0) software, the recording frame rate was 1,200 fps in high-definition during the present study. The camera exposure time was set at 7.98 μs. The video movies were analysed manually to guarantee maximum reliability of the data. The camera was positioned beside the right glass sidewall facing the phase-detection probe array. The observation window was 35 cm wide and 55 cm long, while the depth of field was less than 20 mm. The observations were two-dimensional (Fig. 2), and three-dimensional patterns would not be typically recorded.

High-resolution photographs were taken with a digital SLR camera Pentax™ K-3 (6016×4000 pixels). The camera was equipped with a Voigtlander™ Nokton 58 mm f/1.4 SL II lens, producing images with absolutely negligible degree (~0.31%) of barrel distortion. The camera operated in shutter-priority mode. The shutter speed was set between 1/320 s to 1/8,000 s, corresponding to an exposure time between 3.1 ms and 125 μs respectively.

2.2. Experimental Flow Conditions

The bed particles were randomly placed. Prior to each experimental run, the pebble bed was smoothed, levelled, and lightly compacted using a screed. The gravel bed was then drowned with water to release all trapped air between particles.

The surge was generated by the rapid full closure of the downstream Tainter gate located at x = 14.17 m. The initial flow conditions and gate closure were selected (a) to achieve no sediment motion in the initially steady flow and (b) to generate surges covering a relatively wide range of surge Froude numbers ($1 < Fr_1 < 1.5$) using the same initial flow conditions. The bore Froude number is defined as a function of initial flow conditions and bore celerity: $Fr_1 = (V_1+U)/(gd_1)^{1/2}$. The steady flow was established for at least 3 minutes prior to the measurements and the data sampling started 60 s before gate closure. After each gate closure, the bore propagated upstream against the initially steady flow and the experiment was stopped when the surge front reached the upstream intake structure. Although a number of tests were conducted, detailed velocity and sediment motion observations were performed for one Froude number.

The experimental flow conditions are summarised in Table 1. Velocity and sediment observations were conducted at x = 10.5 m where the boundary layer was fully-developed. The experiments were repeated more than 25 times to ensure the reliability of the ensemble-averaged outcomes (Leng and Chanson 2015). For each experimental run, the video camera and ADV were synchronised mechanically within 0.01-0.05 s.

Table 1. Experimental flow conditions for sediment motion measurements

Reference	Q (m^3/s)	S_o	d_1 (m)	V_1 (m/s)	U (m/s)	Fr_1	Sediment size	Sampling location	Video sampling
Present study	0.061	0	0.161	0.77	1.02	1.42	6.70 - 9.50 mm	x = 10.50 m	1,200 fps
Khezri & Chanson (2012a,b)	0.051	0	0.136	0.75	0.87	1.40	4.75 - 6.70 mm	x = 5.00 m	25 fps
Khezri & Chanson (2015)	0.050	0	0.140	0.71	0.84	1.40	4.75 - 6.70 mm	x = 5.00 m	25 fps

3. Basic Flow Patterns

Following the rapid closure of the Tainter gate, the steady flow was abruptly blocked and reflected to form a positive surge with a sharp front. Visual observation demonstrated that the bore had a breaking roller with strong air entrainment prior to its first crest and small secondary waves. The ensemble-averaged median water depths at different longitudinal locations are presented in Figure 3, where t = 0 corresponds to bore roller toe passage at x = 10.50 m. The newly-generated surge was rapidly detected by the ADM located at x = 13.85 m, that is 0.32 m upstream of the gate location. Further upstream, the secondary wave behind the bore front became stronger. The breaking roller remained but its length became shorter gradually with increasing upstream propagation, as the surge weakened. The type of bore changed progressively from breaking bore to undular bore, in a manner somehow similar to decelerating bore experiments on a slope (Li and Chanson 2017), although the present channel slope was horizontal. The gradual change in bore type was believed to be linked to some energy dissipation and energy transfer to pebble motion. Indeed, during breaking bore passage, Khezri and Chanson (2012c) measured normal Reynolds stresses and turbulent kinetic energy (TKE) on average 10% to 30% higher on a mobile bed than on a fixed bed, at the same relative bed elevation for the same Froude number, throughout the entire water column.

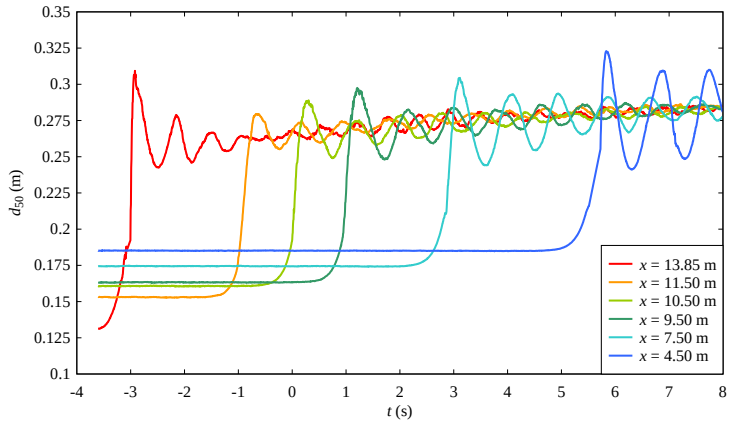

Figure 3. Time evolution of ensemble-averaged median free-surface elevations at different longitudinal locations during tidal bore propagation through the observation section - t = 0 refers to the arrival of the roller toe at the ADV location (x = 10.50 m)

Detailed velocity measurements were conducted at x = 10.50 m with the ADV control volume located at z = 10.8 mm above the top of the pebble layer. Figure 4 illustrates the ensemble-averaged median longitudinal velocity with a reference to the free-surface elevation. Here, V_x was positive downstream, and d_{50} and $(V_x)_{50}$ denote the median data: i.e., ensemble median water depth and ensemble median longitudinal velocity. The passage of the bore front was linked to the abrupt and strong deceleration. The flow reversed its direction immediately with the arrival of roller toe (t = 0) and reached an upstream peak value of about -0.3 m/s. The near-bottom transient fluid recirculation was also observed in field measurements (Mouaze et al. 2010, Reungoat et al. 2015, 2017) and in physical models (Chanson and Docherty 2012, Chanson and Toi 2015). The upstream reversal flow decreased to about -0.1 m/s after the first crest passage, before the longitudinal velocity data showed some undulation linked to the secondary wave motion. This transient recirculation was believed to be a typical characteristic of breaking bores (Khezri and Chanson, 2012b).

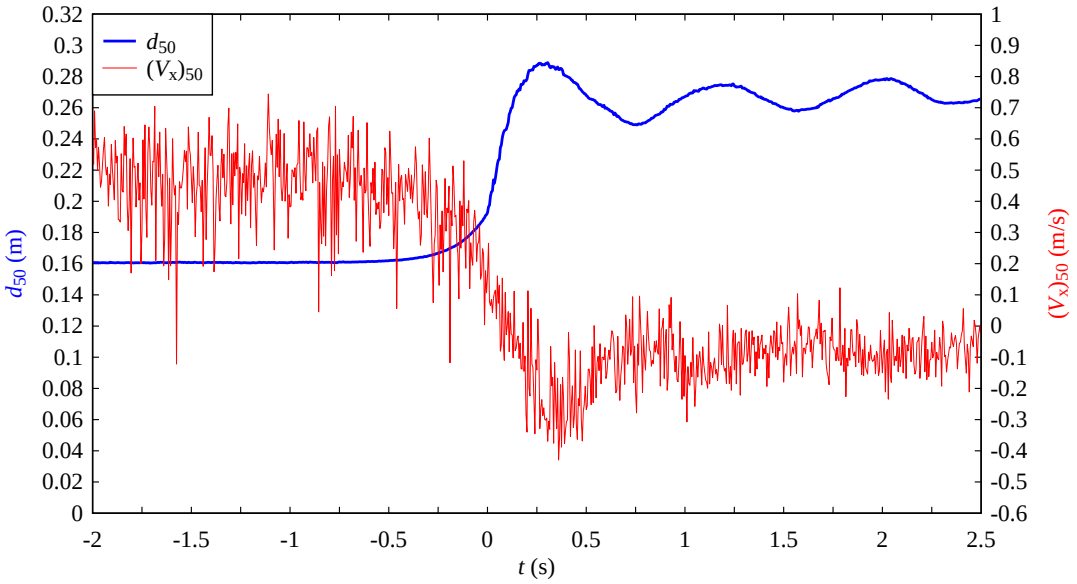

Figure 4. Time evolution of ensemble-averaged median water depth d_{50} and near-bottom longitudinal flow velocity $(V_x)_{50}$ at the ADV location (x = 10.50 m) - t = 0 refers to the arrival of roller toe at the ADV stem

4. Sediment Motion and Transport

4.1. Basic Sediment Motion Patterns

Based upon visual observations and video recordings, no gravel motion was observed in the steady flow prior to the bore passage. With the passage of a breaking bore, some transient upstream gravel transport was seen.

Compared to the experiments of Khezri and Chanson (2012a,b), there was a lesser amount of pebble movement during the bore passage. In their experiments, the transient motion of sediment particles was easily seen in the form of a sudden sheet flow through the whole recording window. Herein, in each video, only about 5 pebbles experienced some upstream motion and changed their positions. The breaking bores in both studies had a similar Froude number $Fr_1 \approx 1.4$, indicating similar bore strength. Two main differences were the composition of movable bed. The mobile bed in Khezri and Chanson (2012a,b) was made of a thin layer (2-3 grain size thick) of loose pebbles distributed over a 1 m long section, with fixed gravel bed upstream and downstream. The mobile bed in the current study was 11.5 m long and 50 mm thick (Fig. 1). Furthermore, the grain size was larger in the present study (Table 1).

The ultra-high-speed video movies at 1200 fps provided fine details of sediment transport in slow motion. For comparison, Khezri and Chanson (2012a,b, 2015) recorded movies at 25 fps. Based on the detailed analysis of the ultra-high-speed videos, the sediment particle motion beneath bores were categorised into 3 basic modes: (1) rotating motion, (2) rolling motion, and (3) saltation motion. A majority of pebbles set into motion experienced a rotating mode (Fig. 5). Figure 5 presents 3 frames of the rotating motion of a dark pebble. In Figure 5, the red dotted line is aligned with the major axis of the particle. For this scenario, the pebble was initially set to rotate counter-clockwise, viewed from the right sidewall, and stopped with a total rotation angle less than 180°. During the rotation process, the pebble did not slide or roll over the surrounding contacting gravels. The rotating pebble remained at the same absolute longitudinal location, or travelled less than one grain size. This motion mode did not contribute to upstream sediment transport during bore passage. The second motion mode is illustrated in Figure 6 by a rolling particle, for which the centre of gravity is marked by red dot. The gravel started its upstream advection with an initial counter-clockwise rolling motion over the surrounding pebbles around the contact point. From its inception to stoppage, the pebble was always in contact with particles in the immediate vicinity and did not suspend in the fluid column. The travelled distance was typically more than two grain sizes (rolling over at least one pebble), with a net-flux of sediment transport in the upstream direction. The saltation motion of a marked pebble is presented in Figure 7 between positions A and B. The inception of sediment movement began at position A and the pebble was immediately lifted up from the contact position with ambient gravels. When suspended in the fluid, the particle in motion travelled upstream in a roughly ballistic trajectory, without grain contact, before its collision with another pebble at position B. This type of pebble motion also contributed to the net-flux of upstream sediment transport.

In practice, once a pebble was set into an upstream motion, its movement was not restricted to the above-mentioned three basic modes. The bed-load motion beneath a bore was usually a combination of two or three kinds of basic motions. Such a combination mode is also shown in Figure 7. After the collision at position B, the pebble continued bouncing in the upstream direction before landing at position C. There the pebble was not set at ease immediately: it laid down after a rotation. Other combination modes (e.g. rolling after saltation) were also observed but not shown here.

The pebble motion was studied within the field of view of the camera. Visual observations showed that the particle trajectories took place mostly within a two-dimensional x-z plane, although it is acknowledged that pebbles could rotate around the x-axis.

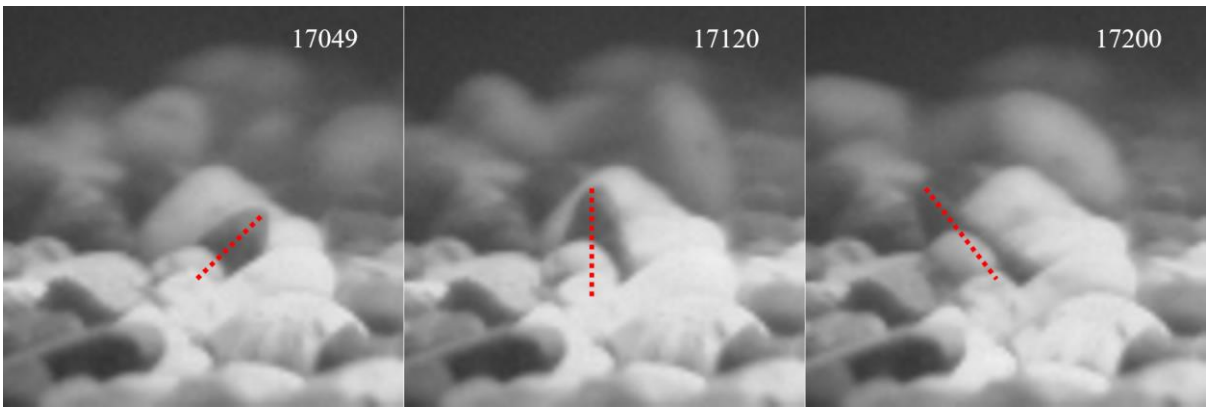

Figure 5. Rotating motion of a pebble during breaking bore passage - snapshots in sequence: from left to right; bore propagation direction: from right to left - Note the red characteristic reference line of the dark pebble; each frame number is marked for video recording at 1200 fps, corresponding to 14.2075 s, 14.2667 s and 14.3333 s from left to right

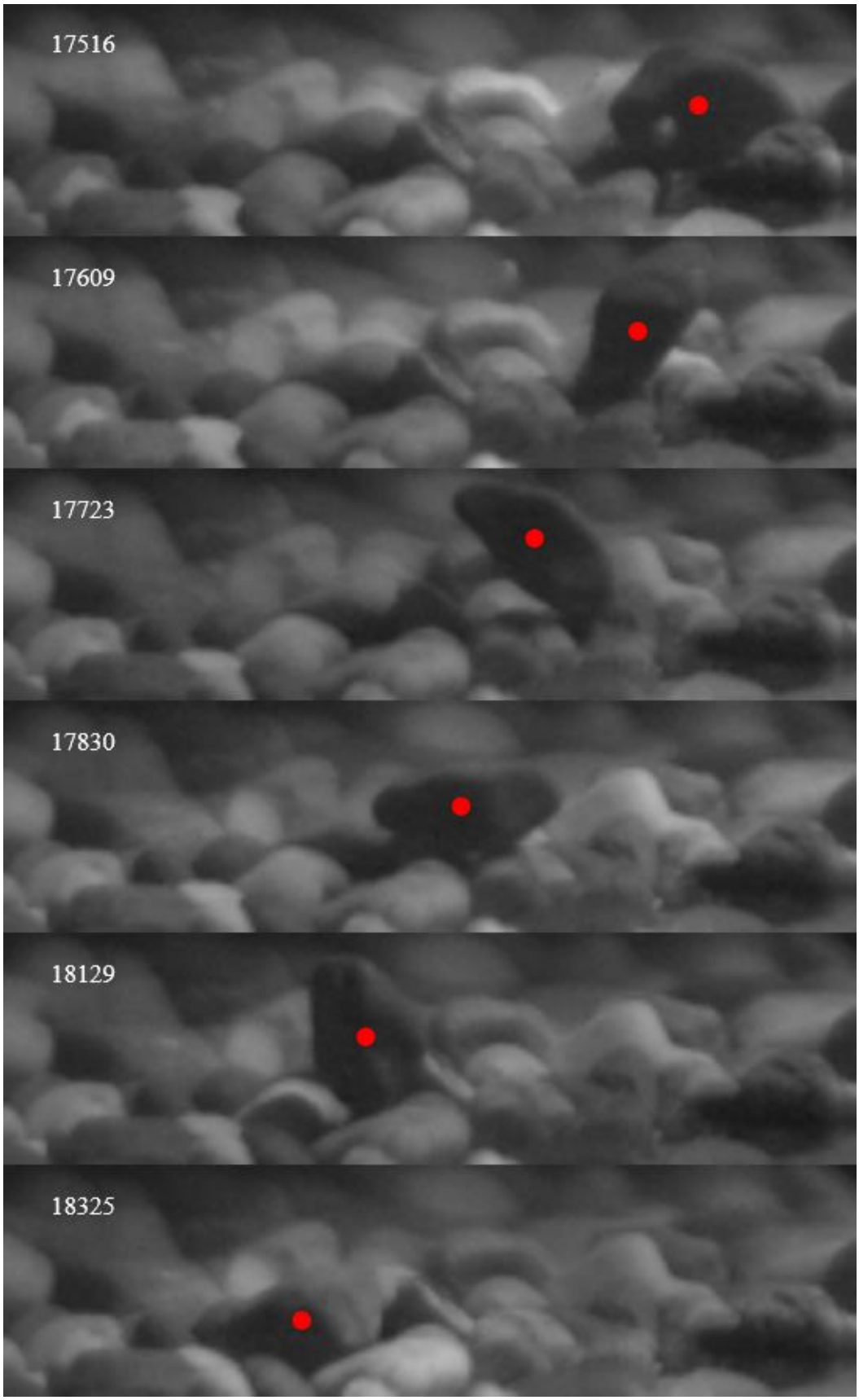

Figure 6. Rolling motion of a pebble (targeted by red dot) during breaking bore passage - snapshots in sequence: from top to bottom; bore propagation direction: from right to left - Each frame number is marked for video recording at 1200 fps, corresponding to 14.5967 s, 14.6742 s, 14.7692 s, 14.8583 s, 15.1075 s, and 15.2708 s from top to bottom

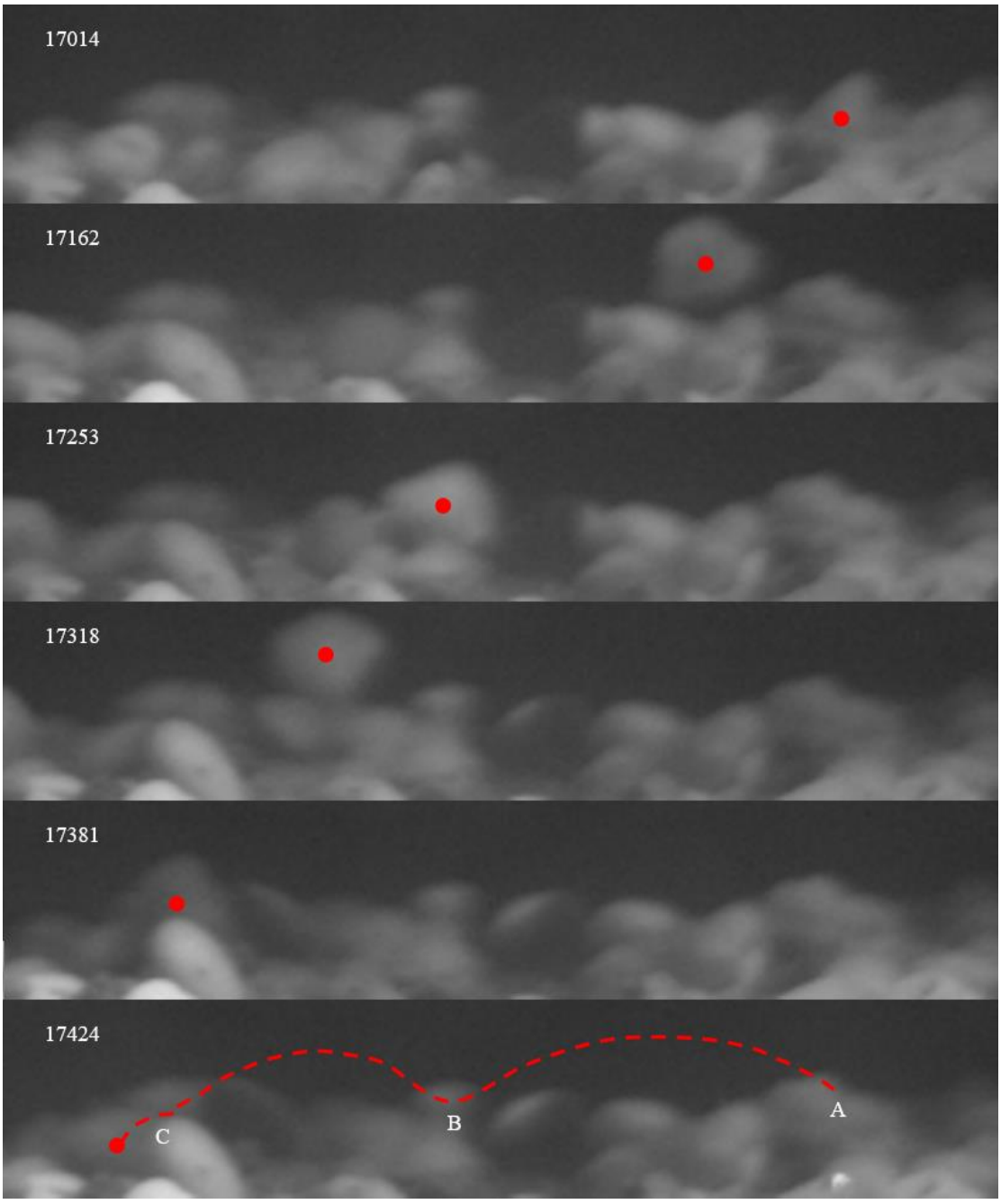

Figure 7. Saltation motion of a pebble (marked by red dot) during breaking bore passage - Bore propagation direction from right to left - Snapshots in sequence from top to bottom - The last snapshot was overlaid with the roughly ballistic trajectory; Each frame number is marked for video recording at 1200 fps, corresponding to 14.1783 s, 14.3017 s, 14.3775 s, 14.4317 s, 14.4842 s, and 14.5200 s

4.2. Sediment Motion Trajectories

The video recording system consisted of Phantom™ v2011 camera controlled by PCC software v2.8.761.0. The software was also capable of analysing the particle motion frame by frame. The sediment motion relative to the breaking bore passage was tracked and compared to roller toe propagation. A typical result is shown in Figure 8a in terms of the centre of gravity of sediment particles: the longitudinal locations of the tracked pebbles (coloured trajectories) and the roller toe position (black line) are plotted as functions of time. Note that the trajectory data were not smoothed. Overall, the inception of bed-load motion (i.e. rolling and/or saltation modes) took place immediately after the roller toe arrival, with a delay less than 0.15 s. It is believed that the upstream particle motion was linked to the combined effects of (a) adverse longitudinal pressure gradient ($\partial P/\partial x < 0$) during the roller toe passage and (b) transient flow reversal next to the bed. In Figure 4, the near-bottom transient flow reversal occurred immediately after the roller toe passage and reached a peak magnitude about 0.3 s later.

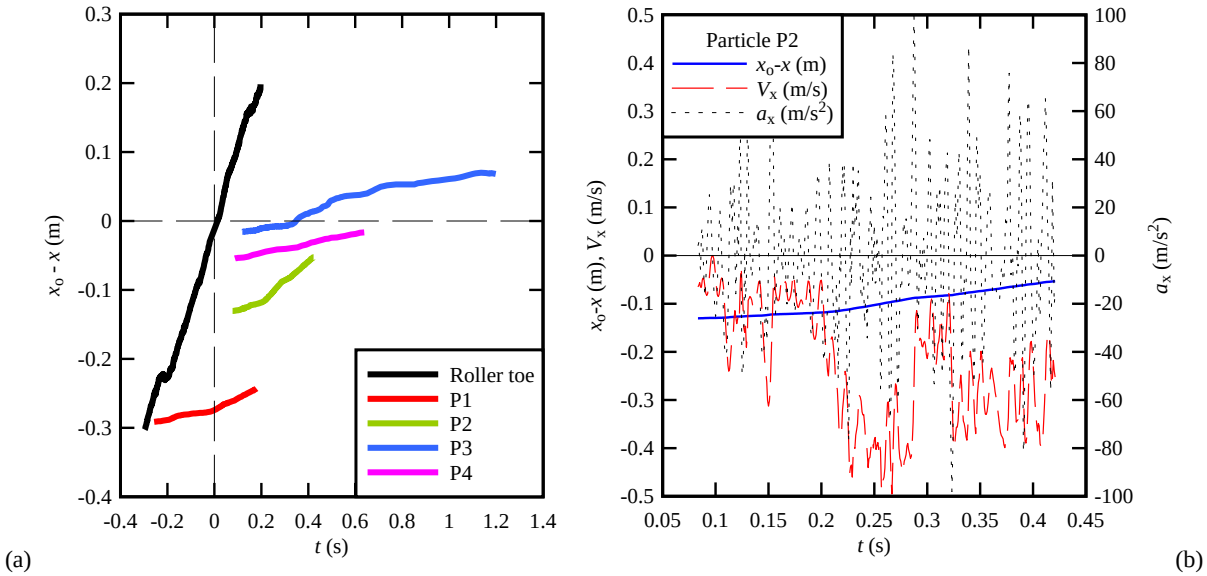

Figure 8. Sediment particle trajectories during a breaking bore passage. (a) Longitudinal trajectories of the sediment particles set to motion (coloured) and the roller toe (black) as functions of time (raw data) - t = 0 refers to the arrival of roller toe at the ADV stem and x_o refer to the longitudinal location of the ADV control volume. (b) Instantaneous longitudinal particle velocity and acceleration (positive downstream) for particle P2

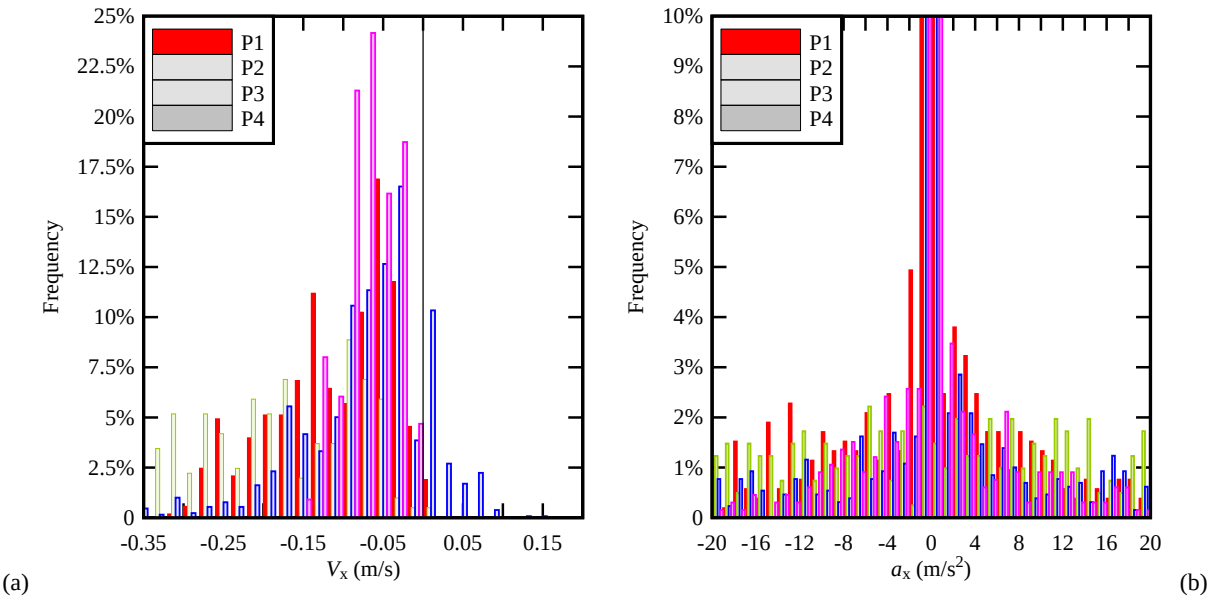

Figure 9. Sediment particle velocity and acceleration probability distribution functions (PDFs) beneath a breaking tidal bore. (a) PDF of instantaneous particle velocities (positive downstream). (b) PDF of instantaneous particle accelerations (positive downstream)

For each particle trajectory shown in Figure 8a, the average upstream particle velocities ranged from -0.07 m/s to -0.25 m/s, the amplitude of which was significantly smaller than the bore celerity -1.05 m/s. However, the pebble velocities were comparable to the peak velocity of the near-bottom transient flow reversal of about -0.3 m/s. The duration of each particle trajectory varied from 0.3 s to 1.1 s, which was relatively long compared the bore front passage. In the particular case of particle P3, the particle stopped travelling upstream about 1.2 s after the roller toe passage. It suggested that the weak negative flow beneath the secondary waves contributed to maintain the upstream particle motion. Despite a smaller data sample and slightly-different boundary conditions (Table 1), the present observations were comparable to the observations of Khezri and Chanson (2012a,2015), in terms of trajectory duration and average particle velocity.

Notwithstanding the limited number of tracked particles, the high recording rate and high-definition of the movies (1,200 fps at 1280×800 pixels) enabled the analyses of instantaneous pebble velocities and accelerations. Missing

data were herein replaced by linear interpolation. Then the trajectory data were smoothed using a 7-point Gaussian filter of standard deviation $\sigma = 3$ (Russ 2011). The velocity and acceleration data were differentiated using a central difference technique. Figure 8b shows typical time-variations of instantaneous longitudinal particle velocity and acceleration (positive downstream). For the data shown in Figure 8a, the histograms of sediment particle velocities and accelerations are shown in Figure 9. The majority of instantaneous particle velocities had an amplitude less than 0.2 m/s (Fig. 9a). The maximum instantaneous value could reach -0.5 m/s. A number of instantaneous velocities were positive: a pebble could move downstream against the bore direction. Such instantaneous downstream velocities of the pebbles were typically linked to the pebble rotating motion in reverse direction, especially before pebble re-stabilisation. The instantaneous pebble accelerations showed symmetrical distribution about zero (Fig. 9b). The acceleration band [-1 to +1] m/s^2 accounted for over 40% of all samples, indicating that the resultant of longitudinal forces acting on a sediment particle was nearly balanced for a majority of time. Instantaneous acceleration magnitudes larger than the gravity acceleration were also observed, as reported by Khezri and Chanson (2015). Herein particle acceleration magnitudes in excess of 20 m/s^2 accounted for nearly 20% of the data sample. The largest accelerationd/decelerations were typically linked to the sediment motion onset, intergranular collisions and stoppage motion.

5. Conclusion and Future Outcomes

The sediment motion beneath a travelling breaking bore was systematically investigated using high-frequency sampling of free-surface elevation and near-bottom flow velocity, in combination to ultra-high-speed video recording. New experiments were conducted over an 11.5 m long 50 mm deep mobile bed, consisting of mixed natural river pebbles (6.7-9.5 mm). The free-surface measurements at several longitudinal locations confirmed the changing bore shape, which was linked to some energy dissipation and energy transfer to pebble motion, during the upstream bore propagation. The ultra-high-speed video recordings at 1,200 fps provided fine details of the upstream gravel particle motion, indicating three basic particle motion modes: rotation, rolling and saltation. More complicated pebble motions were observed, with combinations of two or three basic modes. The simultaneous measurements of free-surface elevation, near-bottom velocity and bed-load transport trajectories highlighted the significance of the combined effect of adverse longitudinal pressure gradient ($\partial P/\partial x < 0$) and transient flow reversal during the bore roller passage, in setting the particles into motion. The long duration of some particle motion suggested some weak negative flow under secondary waves that contributed to maintaining the upstream sediment transport. Both large instantaneous particle velocities and accelerations were derived from the trajectory data. The large particle acceleration could be linked to large transient net force exerted by the fluid on the particles during bore propagation.

The preliminary analysis of current experiment data gave a basic demonstration of sediment transport induced by breaking bores on a mobile gravel bed, as well as of the potential of ultra-high-speed video recording under controlled flow conditions. Further processing of the ultra-high-speed video is required for more detailed statistical outcomes. In particular, more accurate and efficient particle tracking method should be developed to achieve this goal.

6. Acknowledgements

This work was conducted in the AEB hydraulics laboratory at the University of Queensland. The authors are grateful to Dr Hang Wang and Ms Xinqian (Sophia) Leng (The University of Queensland) for their helpful advice. They acknowledge the technical support provided by Jason Van Der Gevel and Stewart Matthews (The University of Queensland). The financial assistance of the Australian Research Council (ARC DP120100481) and China Scholarship Council (CSC) is acknowledged.

7. References

Benet, F. and Cunge, J.A. (1971). "Analysis of experiments on secondary undulations caused by surge waves in trapezoidal channels." *Journal of Hydraulic Research*, IAHR, 9(1), 11-33 (DOI: 10.1080/00221687109500335).

Chanson, H. (2011). "*Tidal Bores, Aegir, Eagre, Mascaret, Pororoca: Theory and Observations*." World Scientific, Singapore.

Chanson, H., and Docherty, N.J. (2012). "Turbulent Velocity Measurements in Open Channel Bores." *European Journal of Mechanics B/Fluids*, 32, 52-58 (DOI 10.1016/j.euromechflu.2011.10.001).

Chanson, H., and Toi, Y.H. (2015). "Physical Modelling of Breaking Tidal Bores: Comparison with Prototype Data." *Journal of Hydraulic Research*, IAHR, 53(2), 264-273 (DOI: 10.1080/00221686.2014.989458)

Cunge, J.A. (1975). "Numerical Methods of Solution of the Unsteady Flow Equations." in *Unsteady Flow in Open Channels.* WRP Publ., Fort Collins, USA, K. Mahmood and V. Yevdjevich Editors, 2, 539-586.

Favre, H. (1935). "*Etude Théorique et Expérimentale des Ondes de Translation dans les Canaux Découverts*." ('Theoretical and Experimental Study of Travelling Surges in Open Channels.') Dunod, Paris, France (in French).

Greb, S.F., and Archer, A.W., (2007). "Soft-sediment deformation produced by tides in a meizoseismic area, Turnagain Arm, Alaska." *Geology*, 35(5), 435-438 (DOI: 10.1130/G23209A.1).

Henderson, F.M. (1966). "*Open Channel Flow*." MacMillan Company, New York, USA.

Khezri, N., and Chanson, H. (2012a). "Inception of Bed Load Motion beneath a Bore." *Geomorphology*, 153-154, 39-47 & 2 video movies (DOI: 10.1016/j.geomorph.2012.02.006).

Khezri, N., and Chanson, H. (2012b). "Sediment Inception under Breaking Tidal Bores." *Mechanic Research Communications*, 41, 49-53 & 1 video movie (DOI: 10.1016/j.mechrescom.2012.02.010).

Khezri, N., and Chanson, H. (2012c). "Undular and Breaking Tidal Bores on Fixed and Movable Gravel Beds." *Journal of Hydraulic Research*, IAHR, 50(4), 353-363 (DOI: 10.1080/00221686.2012.686200).

Khezri, N., and Chanson, H. (2015). "Turbulent Velocity, Sediment Motion and Particle Trajectories under Breaking Tidal Bores: Simultaneous Physical Measurements." *Environmental Fluid Mechanics*, 15(3), 633-651 (DOI: 10.1007/s10652-014-9358-z) & (DOI: 10.1007/s10652-014-9360).

Leng, X., and Chanson, H. (2015). "Unsteady Turbulence in Expansion Waves in Rivers and Estuaries: an Experimental Study." *Environmental Fluid Mechanics*, 15(5), 905-922 (DOI: 10.1007/s10652-014-9385-9).

Leng, X., and Chanson, H. (2016). "Coupling between Free-surface Fluctuations, Velocity Fluctuations and Turbulent Reynolds Stresses during the Upstream Propagation of Positive Surges, Bores and Compression Waves." *Environmental Fluid Mechanics*, Vol. 16, No. 4, pp. 695-719 & digital appendix (DOI: 10.1007/s10652-015-9438-8).

Li, Y., and Chanson, H. (2017). "Free-surface and Velocity Characteristics of Tidal Bore Propagation against a Slope: Experiments on Decelerating Bores." *Proceedings of 37th IAHR World Congress*, IAHR & USAINS Holding Sdn. Bhd. Publ., Kuala Lumpur, Malaysia, 4(3), 3413-3422.

Lighthill, J. (1978). "*Waves in Fluids*." Cambridge University Press, Cambridge, UK.

Mouaze, D., Chanson, H., and Simon, B. (2010). "Field Measurements in the Tidal Bore of the Sélune River in the Bay of Mont Saint Michel (September 2010)." *Hydraulic Model Report No. CH81/10*, School of Civil Engineering, The University of Queensland, Brisbane, Australia, 72 pages.

Reungoat, D., Chanson, H., and Keevil, C.E. (2015). "Field Measurements of Unsteady Turbulence in a Tidal Bore: the Garonne River in October 2013." *Journal of Hydraulic Research*, IAHR, 53(3), 291-301 (DOI: 10.1080/00221686.2015.1021717).

Reungoat, D., Leng, X., and Chanson, H. (2017). "Successive impact of tidal bores on sedimentary processes: Arcins channel, Garonne River." *Estuarine Coastal Shelf Science*, 188, 163-173 (DOI: 10.1016/j.ecss.2017.02.025).

Russ, J.C. (2011). "*The Image Processing Handbook*." CRC Press, Boca Raton, USA.

Stoker, J.J. (1957). "*Water Waves: The Mathematical Theory with Applications*." Interscience Publishers, New York, USA.

Yasuda, H. (2010). "One-dimensional study on propagation of tsunami wave in river channels." *Journal of Hydraulic Engineering*, ASCE, 136(2), 93–105 (DOI: 10.1061/(ASCE)HY.1943-7900.0000150).

Yeow, S.C., Chanson, H., and Wang, H. (2016). "Impact of a large cylindrical roughness on tidal bore propagation." *Canadian Journal of Civil Engineering*, 43(8), 724-734 (DOI: 10.1139/cjce-2015-0557).